ORIGINAL RESEARCH

Development of antiproliferative nanohybrid compound with controlled release property using ellagic acid as the active agent

Mohd Zobir Hussein[1,2]
Samer Hasan Al Ali[2]
Zulkarnain Zainal[2]
Muhammad Nazrul Hakim[3]

[1]Advanced Materials and Nanotechnology Laboratory, Institute of Advanced Technology (ITMA), [2]Department of Chemistry, Faculty of Science, [3]Department of Biomedical Science, Faculty of Medicine and Health Science, Universiti Putra Malaysia, Selangor, Malaysia

Correspondence: Mohd Zobir Hussein
Department of Chemistry, Faculty of Science, Universiti Putra Malaysia, 43400 Serdang, Selangor, Malaysia
Tel +603 89466801
Fax +603 89435380
Email mzobir@science.upm.my

Abstract: An ellagic acid (EA)–zinc layered hydroxide (ZLH) nanohybrid (EAN) was synthesized under a nonaqueous environment using EA and zinc oxide (ZnO) as the precursors. Powder X-ray diffraction showed that the basal spacing of the nanohybrid was 10.4 Å, resulting in the spatial orientation of EA molecules between the interlayers of 22.5° from z-axis with two negative charges at 8,8′ position of the molecules pointed toward the ZLH interlayers. FTIR study showed that the intercalated EA spectral feature is generally similar to that of EA, but with bands slightly shifted. This indicates that some chemical bonding of EA presence between the nanohybrid interlayers was slightly changed, due to the formation of host–guest interaction. The nanohybrid is of mesopores type with 58.8% drug loading and enhanced thermal stability. The release of the drug active, EA from the nanohybrid was found to be sustained and therefore has good potential to be used as a drug controlled-release formulation. In vitro bioassay study showed that the EAN has a mild effect on the hepatocytes cells, similar to its counterpart, free EA.

Keywords: ellagic acid, nonaqueous solution, ZnO, zinc-layered hydroxide, viability test

Introduction

Systemic drug delivery leads to distribution of the drug throughout the body through blood circulation, which can lead to drug concentration accumulation in unwanted parts of the body that causes severe side effects. Additionally, conventional drug administration methods do not provide satisfactory pharmacokinetic profiles because the drug concentration rapidly falls below the desired levels.[1] Cancer chemotherapy is the treatment of cancer cells with an antineoplastic drug. The main property of cancer cells is rapid division. Chemotherapy acts by killing cells that divide rapidly, which means it also harms cells that divide rapidly under normal circumstances such as cells in the bone marrow, digestive tract, and hair follicles, producing side effects such as myelosuppression,[2] mucosities,[3] and alopecia.[4] To overcome these side effects, researchers are now searching for efficient and safe transport carriers, which prolong exposure time to drugs and target cancerous cells without targeting healthy cells.

In the past few decades, many carriers have been developed, and generally can be classified into four major groups: viral carriers, recombinant proteins, organic cationic compounds, and inorganic nanoparticles.[5,6]

Recently, inorganic nanoparticles have attracted considerable attention due to their versatile features, such as wide availability, good biocompatibility, rich surface functionality, potential capability of target delivery, and controlled release of the drug from the inorganic nanoparticles.[7–9] Calcium phosphate, gold, carbon nanotubes, silicon oxide, iron oxide and layered double hydroxides are examples

of inorganic nanoparticles, which have intensively investigated in different studies by different groups.[10–15] Layered double hydroxides (LDH) are materials with a number of advantages for drug delivery. Among these are their ease of laboratory preparation with a controlled particle size,[16] and the drugs can be easily loaded into the interlayers space by ion exchange, comparing with other nanoparticles which need further modification such as surface functional modification.[17,18] Layered double hydroxides have a high zeta potential, 20–30 mV, which provides a strong driving force on to the surface of a cell. LDH are degraded in an acidic environment to form M^{2+}, M^{3+}, and X^- ions which leads the drug actives leaving the cell through the ion-tunnels, whereas the others inorganic nanoparticles accumulate in the cells because of their low solubility in the cells. Low cytotoxicity is another virtue of LDH. Hussein et al reported that there is no toxic effect of Zn–Al LDH at low concentration on Chinese hamster ovary cells.[19]

LDH, also known as hydrotalcite-like compounds, are formed by layered units in which metal cations are octahedrally coordinated with hydroxyl groups, as in the brucite $(Mg(OH)_2)$ structure. The isomorphic substitution of divalent cations by trivalent cations leaves a residual positive charge that is stabilized by inter layer anions. The general formula for hydrotalcite is $\left[M^{2+}_{1-x} M^{3+}_x (OH)_2 \right]^{X+} (A^{m-})_{x/m} \cdot n\,H_2O$, where M^{2+} is divalent cations, M^{3+} is trivalent cations and A^{m-} is exchangeable anion with charge $(m-)$.[20] Similar to LDH, zinc layered hydroxide (ZLH) is a compound whose structure derived from brucite. One quarter of the octahedral coordinated zinc cations are displaced from the main layer to tetrahedral sites located above and below each empty octahedron and can be represented by the general formula $M^{2+}(OH)_{2-x}(A^{m-})_{x/m} \cdot n\,H_2O$, where M^{2+} is the Zn^{2+} and A^{m-} is counter ions with $(m-)$ charge.[21]

Because of ZLH anionic exchange capacity, many active compounds can be intercalated into ZLH interlayers. These include the anticarcinogenic agent gallic acid,[22] linoleic acid,[23] sunscreen materials such as 2-amino benzoic acid and 4-amino benzoic acid,[24] nucleoside monophosphate, DNA,[25] and pharmaceutical, cosmeceutical, and nutraceutical compounds.[26]

Various methods have been adopted for preparation of ZLH and its nanohybrids, namely hydrolysis of salt and oxides,[27] urea hydrolysis,[28] precipitation with alkaline solutions,[29] and solid state reaction.[30] Direct reaction of zinc oxide (ZnO) is simple and easily used either for aqueous or nonaqueous systems. Such a method is economic and environmentally friendly as fewer steps and chemicals are involved.

Ellagic acid (EA) is an antioxidant, which is a family of drugs much used for cancer treatment. Intense research has been conducted to investigate the effect of EA on the cancer cell as well as its delivery.[31–34] Lately, many articles have described the preparation of ZLH as a starting material followed by intercalation of the anion. However, to the best of our knowledge, little work has been published on the use of ZnO as a starting material to intercalate drug actives.[35,36] Therefore, the main objective of this work was to explore the potential use of ZnO as a starting material for the intercalation of EA for the formation of a new EA–ZLH nanohybrid (EAN). The resulting nanohybrid was then used as a controlled release formulation of drug active EA. A cytotoxicity study of nanohybrids was also carried out.

Experimental
Materials
All chemicals used in this study were of analytical grade and used without any further purification. Hydrated EA (97% purity) was purchased from Sigma-Aldrich (St Louis, MO) and pure commercial ZnO of ACS reagent was used, purchased from Fisher Scientific (Waltham, MA). Dimethyl sulfoxide (DMSO) was purchased from Ajax Finechem (Sydney, Australia) with 0.1% water content used as solvent.

Method
Typically, the appropriate amount of hydrated EA (0.0013 mol) was dissolved in DMSO followed by 10 minutes stirring and heating for 40°C. The ZnO (0.2 g) was mixed with the solution of EA and stirred at 70°C for 8 hours. After filtration and washing with deionized water three times, the sample was dried in an oven at 60°C for 12 hours. The resulting material was then powdered and stored in a sample bottle for further use and characterization.

Characterization
Powder X-ray diffraction (PXRD) patterns were recorded at a range of 2–60° on a Shimadzu diffractometer, XRD-6000 (Tokyo, Japan) using CuK_α radiation at 40 kV and 30 mA. Fourier transform infra-red (FTIR) spectra of the materials were recorded over the range 400–4000 cm^{-1} on a Perkin-Elmer 1752X spectrophotometer (Waltham, MA) using a KBr disc method. For carbon, hydrogen, nitrogen and sulfur

Table 1 Physicochemical properties of ZnO and ZLH-nanohybrid, EAN

Compounds	C (%)	H (%)	Zn (%w/w)	[a]Anion (%w/w)	BET surface area (m²/g)	BJH pore diameter (Å)	BJH pore volume (cm³/g)
ZnO	–	–	(80.3)	–	6.4	111	0.010
EAN	32.7	2.6	29.3	58.8	3.6	170	0.007

Notes: [a]Estimated from CHNS analysis; value in the parentheses is the theoretical value.
Abbreviations: BJH, Barret–Joyner–Helenda; BET, Brunauer, Emmett and Teller; C, carbon; H, hydrogen; EAN, ellagic acid nanohybrid; ZnO, zinc oxide; ZLH, zinc layered hydroxide.

(CHNS) analyses, a CHNS-932 model of LECO instrument (St Joseph, MI) was used. Thermogravimetric and differential thermogravimetric analyses (TGA-DTG) were carried out using a Mettler Toledo instrument (Greifensee, Switzerland). Surface characterization of the material was carried out using a nitrogen gas adsorption–desorption technique at 77 K using a Micromeritics ASAP 2000 (Norcross, GA). The surface morphology of the samples was observed by a scanning electron microscope (SEM), using JOEL JSM-6400 (Tokyo, Japan). UV-Vis spectra for optical properties and controlled-release study were accomplished using a Perkin Elmer UV-Vis Spectrophotometer, Lambda 35.

Controlled-release study

Drug release profiles were determined at room temperature by using 0.1 M Na$_2$CO$_3$[37] and Na$_3$PO$_4$[38] solutions. Both anions CO$_3^{-2}$, PO$_4^{-3}$ are commonly used for preliminary study of drug release, to observe the controlled-release property of the intercalated drug actives. This was also conducted to study the effect of different negative species CO$_3^{-2}$, PO$_4^{-3}$ on the rate of release. The UV-Vis spectrum of DMSO and EA dissolved in DMSO shows intense absorbance at 224.0 and 257.5 nm, respectively. Therefore, DMSO is an interference-free solvent. The EA released was measured at a predetermined time by UV-Vis spectrophotometer at 257.5 nm.[39] The EA release kinetics was fitted to four models, as shown in Table 2.[40–43]

In vitro bioassay

The cytotoxicity effect of ZnO, EA, and EAN against healthy rat hepatocytes was examined by a cell viability test. Hepatocytes from normal healthy Sprague Dawley rats (n = 4) were isolated by a two-step collagenase perfusion technique.[44–46] Viability of freshly isolated rat hepatocytes was determined by trypan blue exclusion. After isolation, hepatocytes suspensions were incubated at a density of 1 × 10^6 viable cells/mL in Leibovitz Glutamax I (L-15 incomplete) medium. About 25 µg/mL EA, EAN, and ZnO were added to DMSO (final DMSO concentration of 1.0% v/v). Control hepatocytes suspensions were incubated with an equivalent amount of DMSO. The flasks were sealed in 95% O$_2$/5% CO$_2$ and placed in a shaking water bath at 37°C. Samples were taken from these flasks at time points of 0, 0.5, 1, 3, and 6 hours for a viability test.

Viable cells were determined by lactate dehydrogenase activity in medium and in the lysed cells at each time point. The activity was assessed spectrophotometrically as described by Marshall and Caldwell.[45]

Results and discussion
PXRD and EA orientation between ZLH interlayers

Figures 1A, B, and C show PXRD patterns of ZnO, EAN, and EA, respectively. For ZnO sample, the five intense reflections shown in Figure 1A at 30–60° correspond to

Table 2 Correlation coefficient, rate constant, and half time obtained by fitting the data of the release of EA from EAN into 0.1 M Na$_2$CO$_3$ and 0.1 M Na$_3$PO$_4$; the equation of kinetic models used for the fitting is also indicated

Aqueous solution	Saturated release %	r²				Rate constant (k) pseudo-second order (g/mg·h)	t$_{1/2}$ pseudo-second order (h)
		Zeroth-order	First-order	Pseudo-second order	Parabolic diffusion		
Na$_2$CO$_3$	69%	0.6683	0.7635	0.9985	0.7997	0.0044	3.03
Na$_3$PO$_4$	94%	0.3963	0.7381	0.9996	0.5926	0.0175	0.61
Kinetic equation	Zeroth-order $M_t - M_o = -k_o t$	First-order $\log(M_t/M_o) = -k_1 t$		Pseudo-second order $t/q_t = 1/h + t/q_e$		Parabolic diffusion $(1 - M_t/M_o)/t = K_d t^{-0.5} + a$	

Notes: M$_o$ is the EA content remained in the ZLH at release time o, M$_t$ is the EA content remained in the ZLH at release time t, q$_e$ is the equilibrium release amount and q$_t$ is the release amount at time t, h = k$_2$q$_e^2$, k the corresponding release rate constant, a is constant whose chemical significance is not clearly resolved.[43]
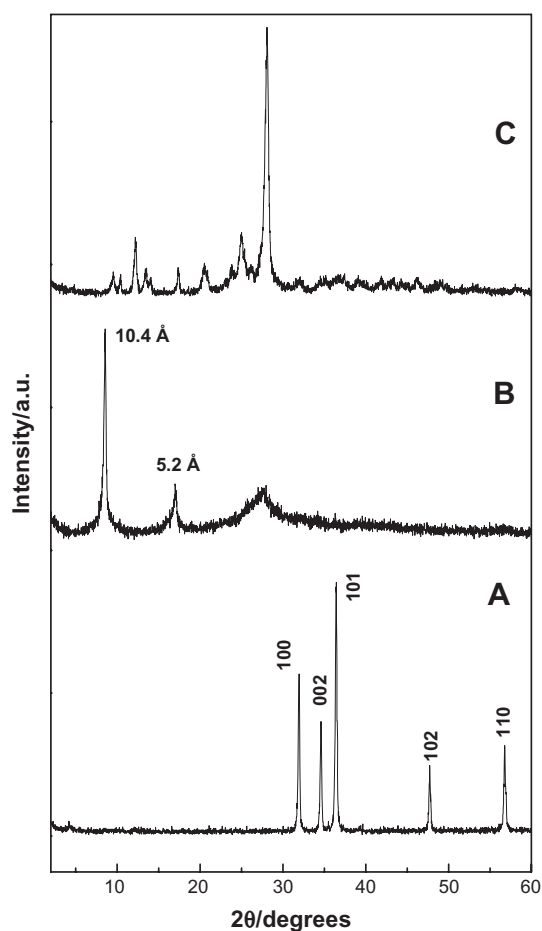**Abbreviations:** EA, ellagic acid; ZLH, zinc layered hydroxide.

**Figure 1** PXRD patterns of ZnO (**A**), EAN (**B**) and EA (**C**).
Abbreviations: PXRD, powder X-ray diffraction; EA, ellagic acid; EAN, ellagic acid nanohybrid.

diffractions due to 100, 002, 101, 102, and 110 planes. Figure 1B shows the PXRD pattern of EAN synthesized by direct reaction between 0.025 M hydrated EA with ZnO. As reported in the literature, the zinc hydroxide nitrate has sharp reflection at 9.7 Å due to the 200 plane of the monoclinic structure.[47,48] After the intercalation of the anions, the basal distance increased more than 9.7 Å due to the displacement

of exchangeable nitrate anions and depending on the dimensions and the spatial orientation of the guest anion that is intercalated into the ZLH inorganic interlayers.[48] As shown in the Figure 1B, the formation of the EAN can be confirmed by the observation of two new diffraction patterns at d = 10.4 Å and 5.2 Å, which is due to 003 and 006 reflection, respectively. Total disappearance of the intense peaks of ZnO phase indicated that the sample EAN is pure phase and the ZnO was completely converted to ZLH.[36]

The formation of EAN is believed to occur through a dissociation–deposition mechanism[36,49] which takes place in the nonaqueous solution of hydrated EA. The mechanism is composed of three steps:
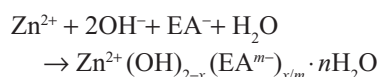
1. Hydrolysis of ZnO in water into hydrated EA to form $Zn(OH)_2$ on the surface of the solid particles

$$ZnO + H_2O \rightarrow Zn(OH)_2$$
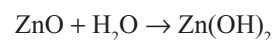
2. Formation Zn^{2+} species by dissociation of $Zn(OH)_2$

$$Zn(OH)_2 \rightarrow Zn^{2+} + 2OH^-$$
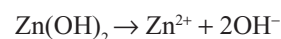
3. In addition, reaction between Zn^{2+} ions formed with hydroxyls, H_2O and EA anions in the solution generate the layered nanohybrid compound,

$$Zn^{2+} + 2OH^- + EA^- + H_2O$$
$$\rightarrow Zn^{2+}(OH)_{2-x}(EA^{m-})_{x/m} \cdot nH_2O$$

The EA has the molecular structure of a planar phenolic lactone that is doubly deprotonated at positions 8 and/or 8′ when the pH is more than 5.6.[50] Figure 2A shows the three-dimensional molecular size of EA obtained using Chemoffice software (Cambridge, MA).

Figure 2B shows that the thickness of the ZLH is 4.8 Å[51] and d-spacing of the ZLH samples intercalated by EA from XRD spectrum is 10.4 Å. Therefore, the gallery height aviamble to be occupied is 5.6 Å, which is smaller than 12.4 Å or 9.8 Å, the dimension of EA. In addition, the thickness of two molecules of EA is about 5.8 Å, which is
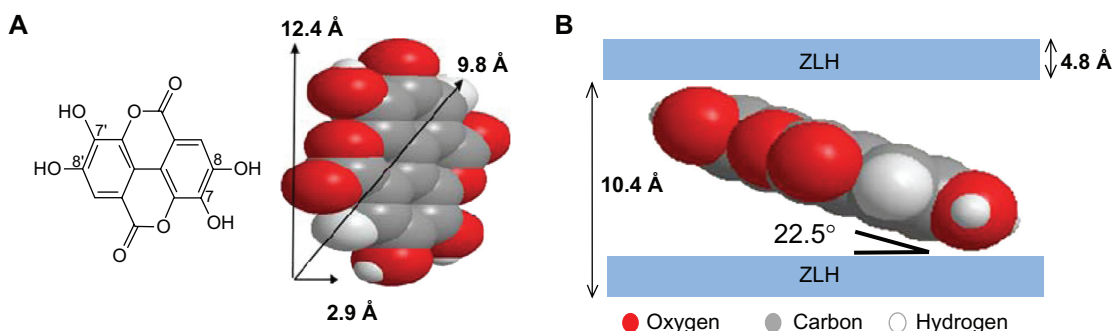

Figure 2 Molecular structure of EA and three-dimensional molecular size of EA (**A**) and spatial orientation of EA in ZLH inorganic interlayers (**B**).
Abbreviations: EA, ellagic acid; ZLH, zinc layered hydroxide.

bigger than the gallery height. This means that the EA has to be oriented between the interlayers as a monolayer and the spatial orientation of the molecule is with an angle of 22.5° from z-axis as shown in Figure 2B.

FTIR spectroscopy

The FTIR spectra of the EAN nanohybrid and EA are given in Figure 3. The FTIR spectrum of EA shows an absorption band at 3557 cm^{-1}, attributed to the stretching mode of OH groups in the phenol at 7,7′, 8 and 8′ positions (Figure 2A)[52] and broad absorption bands at 3500–2750 cm^{-1} can be attributed to stretching of C–H aromatic ring[24] and hydrogen bond between EA molecules.[50] A band at 1700 cm^{-1} is due to stretching of C=O[52,53] and bands at 1620–1511 cm^{-1} are due to aromatic rings. A band at 1196 and 1058 cm^{-1} is due to ester linkage of C–O stretching[34,52] and another band at 758 cm^{-1} is due to C–H aromatic stretching.

FTIR spectrum of EAN (Figure 3B) shows characteristic bands of pure EA together with other band of ZLH. This indicates that the EA has been intercalated into the interlayer galleries of ZLH. Band for C=O, C–O ester linkage and C–H aromatic are slightly shifted in position to 1689, 1064, 750 cm^{-1}, respectively, due to the interaction between EA and the host interlayers as a result of the intercalation process. A broad absorption band observed at 2500–3600 cm^{-1} is attributed to OH stretching due to the presence of hydroxyl group within the ZLH and phenolic hydroxide at position 7,7′.[50] A band at 1577 cm^{-1} can be attributed to C=C stretching vibration of aromatic,[52] and a band for ν(C–O) can be observed at 1107 cm^{-1} and ν(Zn–O) absorption bands at 472 cm^{-1}. This indicates that the EA is coordinated to the inorganic layers by the negatively charged oxygen atoms at positions 8 and 8′.[50,54] The successful intercalation of EA into ZLH can be supported by CHNS analysis as shown in Table 1. EAN shows 32.7% carbon (w/w) and 2.6% (w/w) hydrogen, resulted in loading percentage of EA in the nanohybrid of about 58.8%. Elemental analysis using ICP/AES shows EAN contains 29.3% Zn (w/w).
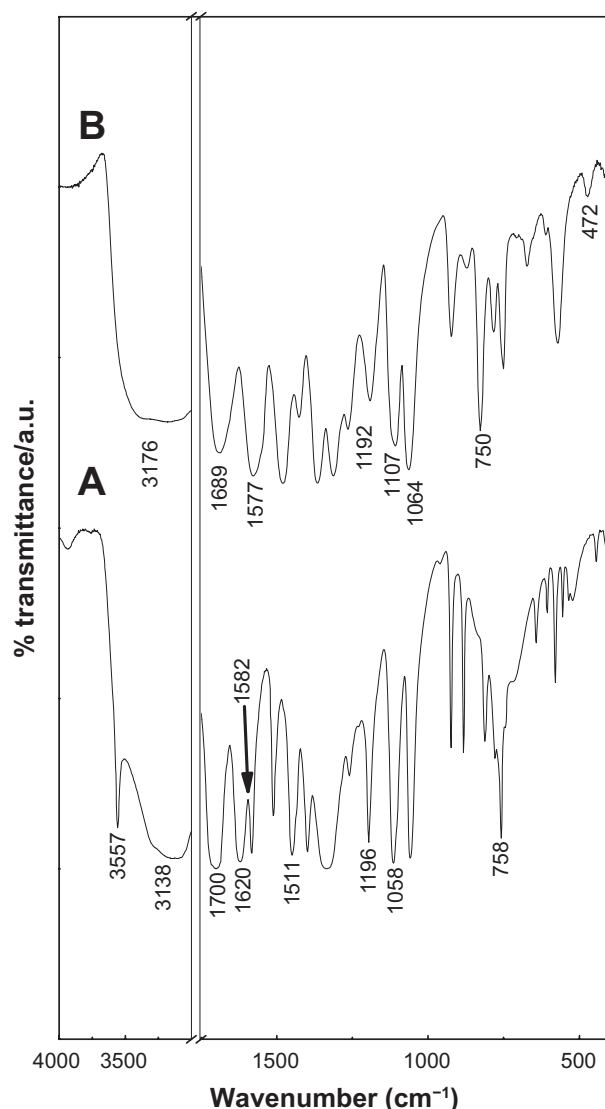
Thermal analysis

TGA-DTG thermogravimetric analysis obtained for EA and EAN is shown in Figure 4. The TGA-DTG thermograms of EA (Figure 4A) show the first step weight loss, which can be attributed to the removal of bonded water with hydrogen bond at temperature maxima of 112°C (8.2%). The onset of weight loss of EA occurs at 381°C with two steps weight loss at 463°C (39%) and 596°C (17.5%). Because of the intercalation, the shape of the TGA-DTG curves (Figure 4B) is changed. The first weight loss at 78°C in the DTA curve corresponding to the absorbed water. The absence of a band at 1600 cm^{-1} in the FTIR spectrum confirming the absence of water between the interlayers.[55] The onset of dehydroxylation of zinc hydroxide layers and decomposition of EA occurs at around 496°C, with a rapid weight loss occurring in the temperature range at 496°C–819°C with two steps at 585°C (24%) and 714°C (25.2%). These temperatures are higher than the decomposition temperature of pure EA. This result indicates that the inorganic layers of ZLH enhanced the thermal stability of EA, the organic moiety.
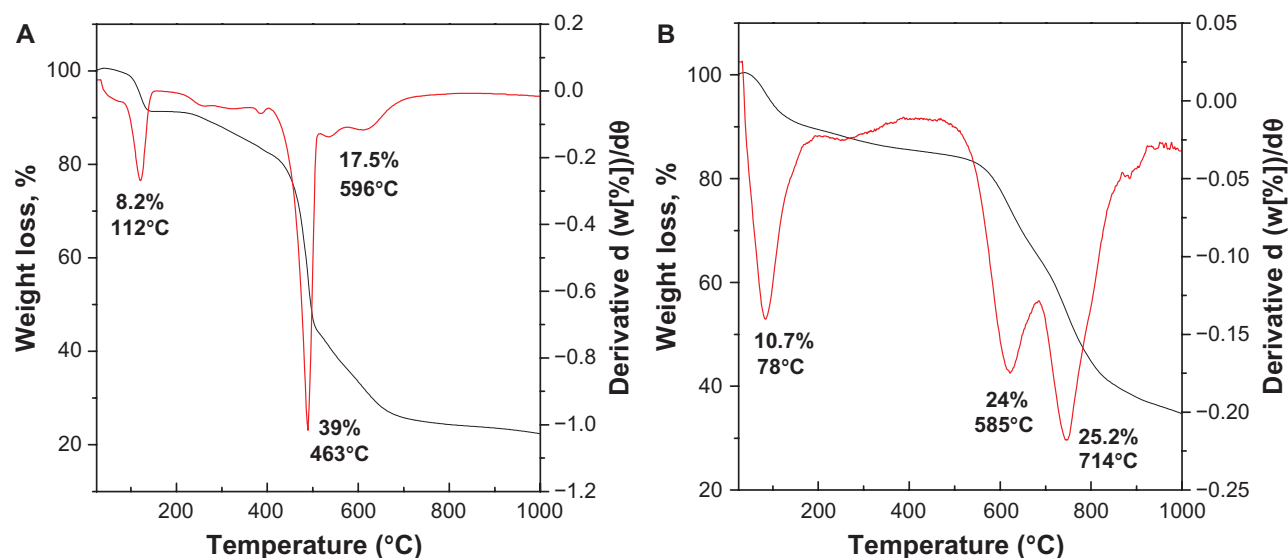

Figure 3 FTIR spectrum of EA (**A**) and EAN (**B**).
Abbreviations: FTIR, Fourier transform infra-red; EA, ellagic acid; EAN, ellagic acid nanohybrid.

Figure 4 TGA-DTG thermogravimetric analysis of EA (**A**) and EAN (**B**).
Abbreviations: TGA–DTG, thermogravimetric and differential thermogravimetric analyses; EA, ellagic acid; EAN, ellagic acid nanohybrid.

Surface properties

Nitrogen adsorption–desorption isotherm for ZnO and EAN are shown in Figure 5A, shows features which can be described as Type IV in IUPAC classification, indicating mesopores-type material.[56] The adsorption of ZnO and EAN increased slowly at low pressure in the range of 0.0–0.8, followed by rapid adsorption of the absorbent at relative pressure of 0.8 and above. The desorption branch of the hysteresis loop for ZnO is much narrower compared to EAN, indicating different pore texture of the resulting materials. This is due to the formation of ZLH with a basal spacing of

10.4 Å as well as the formation of interstitial pores.[57] As a result of nitrogen adsorption study, we obtained the Breuneur, Emmet, and Teller (BET) surface area of the materials as shown in Table 1. The intercalation of EA into ZLH for the formation of EAN resulting in the decrease of the surface area from 6.4 m^2/g for ZnO to 3.6 m^2/g for EAN. This is attributed to the increase in the particles size and decrease of the pore volume.

Barret-Joyner-Halenda (BJH) pore size distribution for ZnO and EAN are shown in Figure 5B. Both materials show mesopores character, in agreement with the adsorption
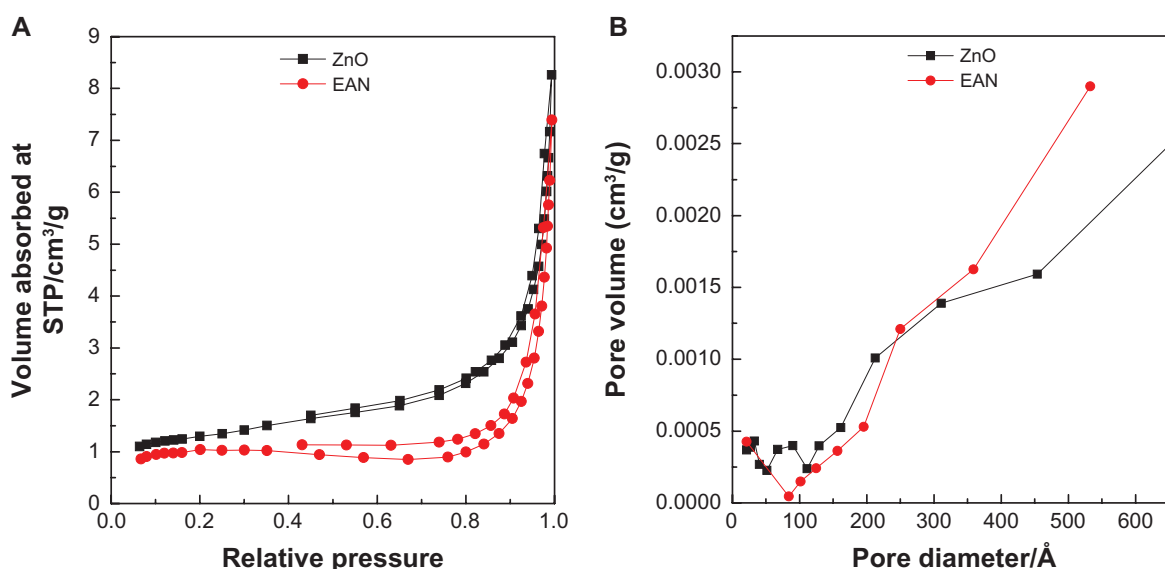

Figure 5 Adsorption–desorption isotherms (**A**) and BJH pore size distribution (**B**) for ZnO and EAN.
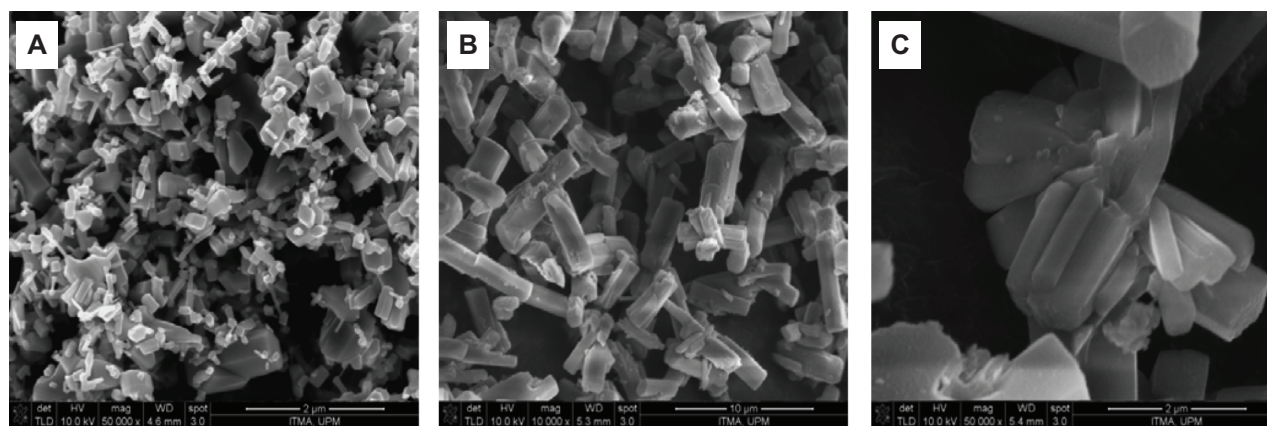**Abbreviations:** BJH, Barret–Joyner–Halenda; EAN, ellagic acid nanohybrid.

Figure 6 FESEM image of ZnO (**A**) and EAN (**B**) and EAN at higher magnification (**C**).
Abbreviations: FESEM, field emission scanning electron microscope; EA, ellagic acid; EAN, ellagic acid nanohybrid.

isotherm of Type IV. BJH pore size distribution of ZnO (Figure 5B) shows different features to that of EAN, indicating that the pore texture was modified, which is in agreement with the formation of EAN with a basal spacing of 10.4 Å. The BJH pore diameter of ZnO is lower than that of EAN. The increase from 111 to 170 Å is as a result of the intercalation of EA into the interlayer of ZLH.

Surface morphology of the samples, studied by field emission SEM for ZnO and EAN are shown in Figure 6. ZnO reveals nonuniform granular structure without any specific shape, with various sizes and shapes (Figure 6A). This structure was transformed into rod-like agglomerates with nonuniform size and shapes as shown in Figures 6B–C, when the intercalation of EA into the interlayer of ZLH had taken place.

Optical properties

UV-Vis spectroscopy was used to investigate whether the intercalation of EA into the ZLH host resulted in changes in its optical properties. Figure 7A shows the UV-Vis spectra of pristine EA as well as EAN. It can be seen that pristine EA exhibits a strong absorption band at 350 nm with a shoulder at 370 nm, corresponding to the $\pi \rightarrow \pi^*$ transition of EA. When EA was intercalated into ZLH interlayers, the 370 nm band was slightly increased in intensity, indicating doubly deprotonated EA between the interlayers.[50] This verifies that the drug molecules are stabilized by electrostatic interaction with the positive charge of ZLH.

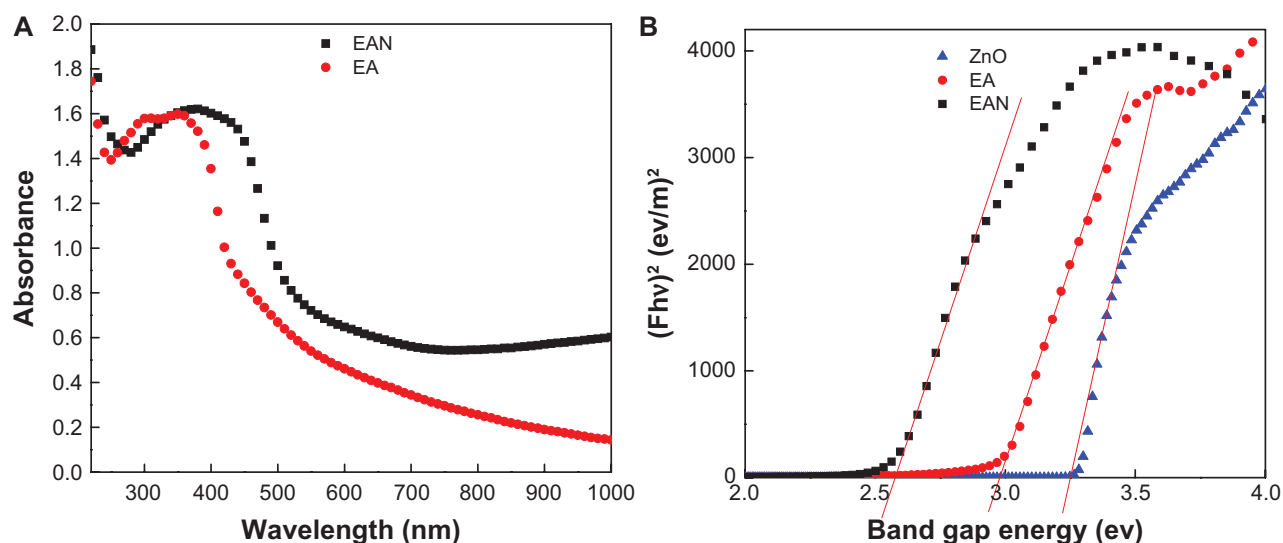In order to estimate the energy band gap, the Kubelka–Munk (K–M) equation (1) was adopted,[58]

Figure 7 Solid-state UV-Vis spectra of pure EA and its nanohybrid, EAN (**A**) and their Kubelka-Munk plot of EA, EAN and ZnO (**B**).
Abbreviations: EA, ellagic acid; EAN, ellagic acid nanohybrid.

$$(F \cdot h\nu)^2 = A(h\nu - E_g) \qquad (1)$$

where F is the K–M, h is Bohr constant, E_g is the energy band gap in electron volt units.

It is clear from Eq. (1) that the band gap can be obtained by plotting $(F \cdot h\nu)^2$ against $h\nu$ in electron volts. Using the data obtained from Figure 7B, the band gap energy, E (eV) was determined, which is 3.29, 2.55, and 2.95 eV for ZnO, EAN, and EA, respectively. The value of band gap for ZnO determined in this work is similar to a band gap energy for ZnO determined previously.[59]

Release behavior of the EA

The release profiles of EA from EAN using 0.1 M Na_2CO_3 and 0.1 M Na_3PO_4 separately and free EA are shown in Figure 8. As can be seen from Figures 8C and D, the free EA released quickly into Na_2CO_3 and Na_3PO_4 solutions, the release being
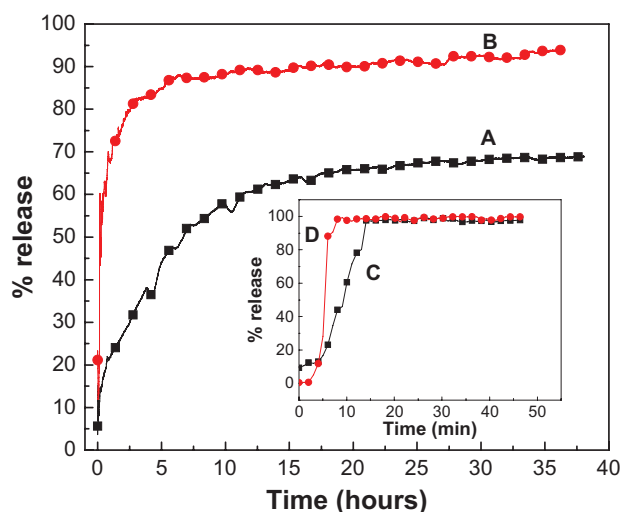

Figure 8 Release profiles of EA from the EAN in the aqueous solution containing 0.1 M Na_2CO_3 (**A**) and 0.1 M Na_3PO_4 (**B**). Inset shows release of free EA into Na_2CO_3 (**C**) and Na_3PO_4 (**D**).
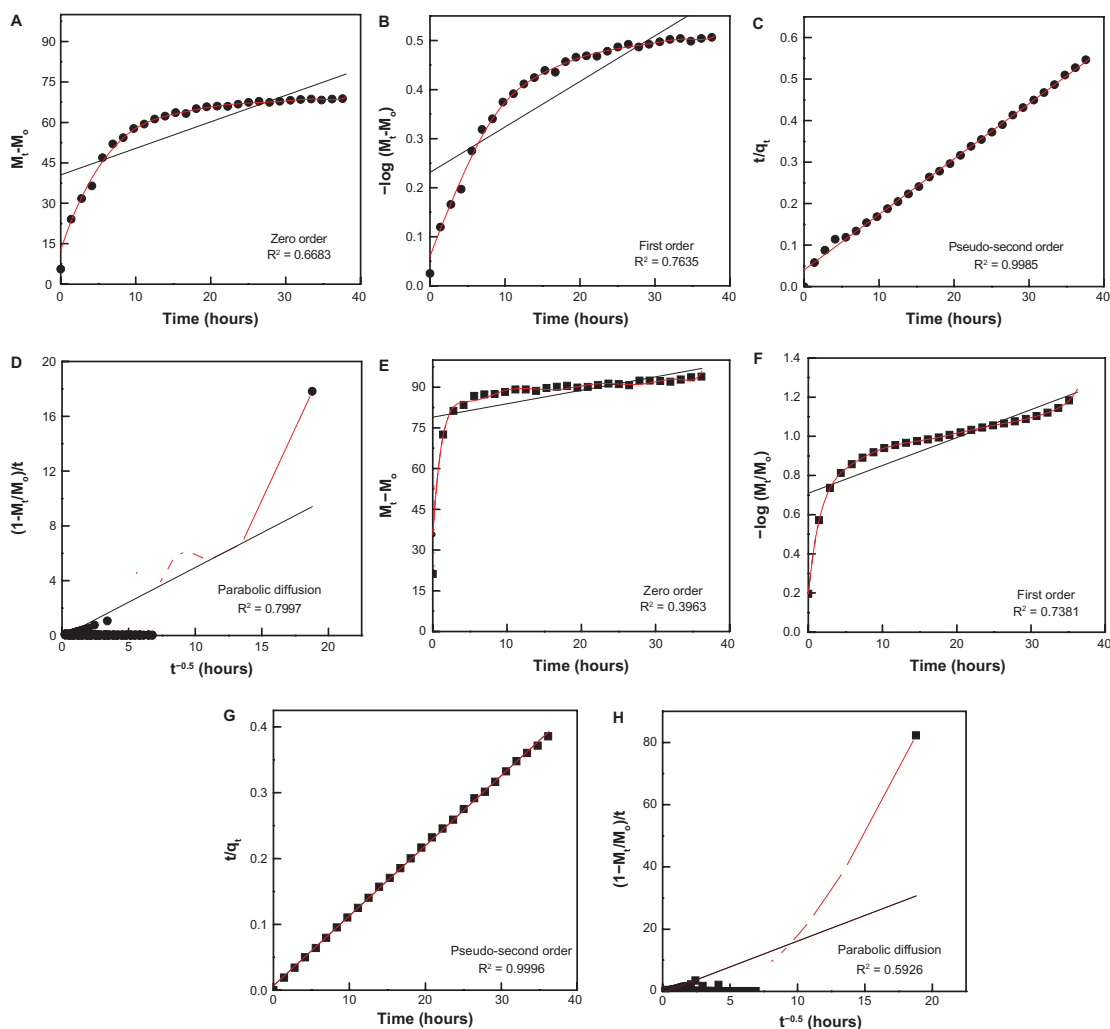**Abbreviations:** EA, ellagic acid; EAN, ellagic acid nanohybrid.

Figure 9 Fitting of the data of EA released from the EAN into solution to the zeroth-, first-, pseudo-second-order kinetics, and parabolic diffusion for 0.1 M Na_2CO_3 (**A**, **B**, **C**, and **D** respectively) and Na_3PO_4 (**E**, **F**, **G**, and **H**, respectively).
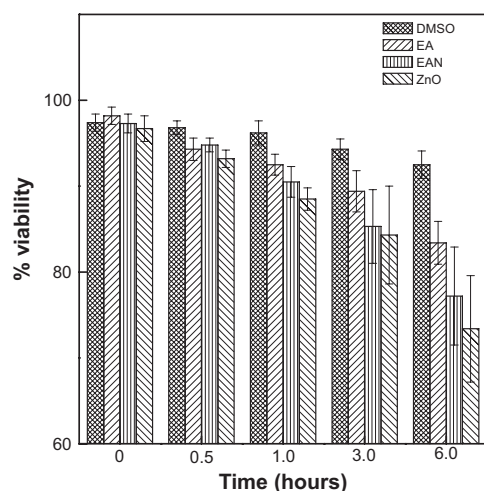**Abbreviations:** EA, ellagic acid; EAN, ellagic acid nanohybrid; ZnO, zinc oxide.

Figure 10 The effect of EA, EAN, and ZnO on the viability of rat hepatocyte cells at the concentration of 25 µg/mL.
Abbreviations: EA, ellagic acid; EAN, ellagic acid nanohybrid; ZnO, zinc oxide.

completed within 26 and 18 minutes in Na_2CO_3 and Na_3PO_4, respectively. The release rate of EA from EAN is obviously lower than the free EA, indicating that the EAN is a potential controlled-release drug system. The release of EA from the nanohybrid is obviously dependent on the types of anion in aqueous solution for ion exchange. It is worth noting that the rapid release during the first 5 hours is followed by a more sustained release of the EA, and 44% and 85% of EA was released from ZLH by Na_2CO_3 and Na_3PO_4 aqueous solution, respectively. A slower release was observed from 5 to 38 hours. The amount of EA released from EAN into aqueous solutions containing Na_3PO_4 was found to be higher than the Na_2CO_3, as shown in Figure 8B. The amount of EA released from the aqueous solution at 38 hours was 94% (Table 2 and Figure 8) for Na_3PO_4 compared with about 69% for Na_2CO_3. Because we know that the more negative charge of phosphate anion will give a higher affinity for ion exchange with the intercalated EA anion, more release of EA is expected, and this is parallel to the release profiles observed in Figure 8.

In order to obtain more information on the release behavior of EA from EAN, zeroth-, first-, pseudo-second-order kinetics and parabolic diffusion, were chosen to investigate

the release kinetics of EA from the nanohybrid. The equations are given in Table 2. On the basis of the four models, the fitted results of EA release profiles are given in Figure 9 and Table 2. It can be seen that the pseudo-second-order model can be better fitted to the data of the EA release behavior than the other models. Figures 9C and G show the plots of t/q_t versus t for the release of EA into Na_2CO_3 and Na_3PO_4 solution, respectively. For the Na_2CO_3, the correlation coefficient (R^2) and k valves are 0.9985 and 0.0044, respectively, compared with 0.9996 and 0.0175, respectively for Na_3PO_4. The saturated release amount, correlation coefficient (R^2) and rate constant for pseudo-second-order model are also given in Table 2. This study indicates that EAN synthesized in this work shows controlled-release properties.

In vitro bioassay

Figure 10 and Table 3 show the effect of free EA, EAN, and ZnO on the viability, using rat hepatocytes cells at various incubation times of 0, 0.5, 1, 3 and 6 hours and at a concentration of 25 µg/mL. As shown in Figure 10, EA has a mild cytotoxic effect on the viability of the hepatocyte cells, similar to ZnO. Interestingly, the EAN also has a mild effect on the hepatocyte cells similar to that of free EA.

A closer look at Table 3 shows no significant toxic effect of EAN on the rat hepatocytes cells up to 6 hours, which indicates that EAN can be further used in the study using cancer cell lines.

Conclusion

This study shows that EA can be intercalated into the interlayer of ZLH under nonaqueous environment by direct reaction with ZnO for the formation of organic–inorganic nanohybrid. The resulting nanohybrid was obtained using 0.025 M EA. The obtained nanohybrid shows a basal spacing of 10.4 Å, which confirms the successful intercalation of EA into the interlayer of ZLH. In addition, FTIR and elemental analyses (CHNS) studies supported the intercalation of EA into ZLH interlayers for the nanohybrid formation, EAN. It was also found that the

Table 3 Viability of hepatocytes during incubation with EA and EAN

	0 h	0.5 h	1.0 h	3.0 h	6.0 h
Control (1% DMSO)	97.4 ± 1.0[aw]	96.8 ± 0.8[aw]	96.2 ± 1.4[aw]	94.3 ± 1.2[aw]	92.5 ± 1.6[ax]
25 µg/mL EA	98.2 ± 1.0[aw]	94.3 ± 1.3[ax]	92.5 ± 1.2[bx]	89.4 ± 2.4[by]	83.4 ± 2.5[by]
25 µg/mL EAN	97.3 ± 1.1[aw]	94.8 ± 0.8[ax]	90.5 ± 1.8[by]	85.3 ± 4.3[bz]	77.2 ± 5.7[cz]
25 µg/mL ZnO	96.7 ± 1.5[aw]	93.2 ± 1.0[bx]	88.5 ± 1.3[cy]	84.3 ± 5.7[by]	73.4 ± 6.2[cz]

Notes: N = 3. Values are mean ± SD. Means with different superscript (a–c) differs significantly ($P < 0.05$) by ANOVA and Duncan multiple post-test in the same column and (w–z) differs significantly in the same row.
Abbreviations: EA, ellagic acid; EAN, ellagic acid nanohybrid; ZnO, zinc oxide.

BET surface area declined from 6.4 to 3.6 m²/g when ZnO is transformed to EAN. The high loading of EA molecules inside the interlayers of about 58.8% is useful for controlled-release purposes, and the controlled-release study showed the drug active, EA was released in a controlled manner. The EAN has a mild effect on the hepatocyte cells similar to its counterpart, free EA, which indicates that the EAN can be further used in the study on cancer cell lines.

Acknowledgment

Disclosure

The authors declare no conflicts of interest in this work.

References

1. Trikeriotis M, Ghanotakis DF. Intercalation of hydrophilic and hydrophobic antibiotics in layered double hydroxides. *Int J Pharm*. 2007;332(1–2): 176–184.
2. Ari ZB, Mehta A, Lennard L, Burroughs AK. Azathioprine-induced myelosuppression due to thiopurine methyltransferase deficiency in a patient with autoimmune hepatitis. *J Hepatol*. 1995;23(3):351–354.
3. Tanner NS, Stamford IF, Bennett A. Plasma prostaglandins in mucositis due to radiotherapy and chemotherapy for head and neck cancer. *Br J Cancer*. 1981;43(6):767–771.
4. Rosman S. Cancer and stigma: experience of patients with chemotherapy-induced alopecia. *Patient Educ Couns*. 2004;52(3):333–339.
5. Azzam T, Domb AJ. Current developments in gene transfection agents. *Curr Drug Deliv*. 2004;1(2):165–193.
6. Garnett MC. Gene-delivery systems using cationic polymers. *Critical Rev Ther Drug Carrier Syst*. 1999;16(2):147–207.
7. Barbé C, Bartlett J, Kong L, et al. Silica particles: a novel drug-delivery system. *Adv Mater*. 2004;16(21):1959–1966.
8. Bauer LA, Birenbaum NS, Meyer GJ. Biological applications of high aspect ratio nanoparticles. *J Mater Chem*. 2004;14(4):517–526.
9. Ozkan M. Quantum dots and other nanoparticles: what can they offer to drug discovery? *Drug Discov Today*. 2004;9(24):1065–1071.
10. Cheng X, Kuhn L. Chemotherapy drug delivery from calcium phosphate nanoparticles. *Int J Nanomedicine*. 2007;2(4):667–674.
11. Shenoy D, Fu W, Li J, et al. Surface functionalization of gold nanoparticles using hetero-bifunctional poly (ethylene glycol) spacer for intracellular tracking and delivery. *Int J Nanomedicine*. 2006;1(1):51–57.
12. Popov AM, Lozovik YE, Fiorito S, Yahia LH. Biocompatibility and applications of carbon nanotubes in medical nanorobots. *Int J Nanomedicine*. 2007;2(3):361–372.
13. O'Farrell N, Houlton A, Horrocks BR. Silicon nanoparticles: applications in cell biology and medicine. *Int J Nanomedicine*. 2006;1(4):451–472.
14. Wu X, Tan Y, Mao H, Zhang M. Toxic effects of iron oxide nanoparticles on human umbilical vein endothelial cells. *Int J Nanomedicine*. 2010;5:385–399.
15. Xu ZP, Walker TL, Liu K, Cooper HM, Lu GQM, Bartlett PF. Layered double hydroxide nanoparticles as cellular delivery vectors of supercoiled plasmid DNA. *Int J Nanomedicine*. 2007;2(2):163–174.
16. Xu ZP, Lu GQ, Max N. Hydrothermal Synthesis of Layered Double Hydroxides (LDHs) from Mixed MgO and Al₂O₃: LDH Formation Mechanism. *Chem Mater*. 2005;17(5):1055–1062.

17. Liu X, Worden JG, Dai Q, Zou J, Wang J, Huo Q. Monofunctional gold nanoparticles prepared via a noncovalent interaction based solid phase modification approach. *Small*. 2006;2(10):1126–1129.
18. Berriozabal G, de Miguel YR. Synthesis and characterisation of silica nanoparticles bearing different functional groups obtained via a two stage method. *Physica Status Solidi C*. 2010;7(11–12): 2692–2696.
19. Ajat M, Mohd M, Yusoff K, Hussein MZ. Synthesis of glutamate-zinc-aluminium-layered double hydroxide nanobiocomposites and cell viability study. *Curr Nanosci*. 2008;4(4):391–396.
20. Rives V. *Layered Double Hydroxides: Present and Future*. New York: Nova Science Pub Inc; 2001.
21. Arizaga GGC, Satyanarayana KG, Wypych F. Layered hydroxide salts: synthesis, properties and potential applications. *Solid State Ionics*. 2007;178(15–18):1143–1162.
22. Hussein MZ, Ghotbi MY, Yahaya AH, AbdRahman MZ. Synthesis and characterization of (zinc-layered-gallate) nanohybrid using structural memory effect. *Mater Chem Phys*. 2009;113(1):491–496.
23. Choy JH, Shin J, Lim SY, Oh JM, Oh MH, Oh S. Characterization and stability analysis of ZnO nanoencapsulated conjugated linoleic acid. *J Food Sci*. 2010;75(6):N63–N68.
24. Cursino ACT, Gardolinski J, Wypych F. Intercalation of anionic organic ultraviolet ray absorbers into layered zinc hydroxide nitrate. *J Colloid Interface Sci*. 2010;347(1):49–55.
25. Choy JH, Kwak SY, Park JS, Jeong YJ, Portier J. Intercalative nano-hybrids of nucleoside monophosphates and DNA in layered metal hydroxide. *J Am Chem Soc*. 1999;121(6):1399–1400.
26. Hwang SH, Han YS, Choy JH. Intercalation of functional organic molecules with pharmaceutical, cosmeceutical and neutraceutical functions into layered double hydroxides and zinc basic salts. *Bulletin-Korean Chemical Society*. 2001;22(9):1019–1022.
27. Rouba S, Rabu P, Drillon M. Synthesis and characterization of new quasi-one-dimensional Mn(II) hydroxynitrates (Mn$_x$Zn$_{1-x}$)(OH)(NO₃) H₂O (x = 0.53, 1.00). *J Solid State Chem*. 1995;118(1):28–32.
28. Stahlin W, Oswald HR. The crystal structure of zinc hydroxide nitrate, Zn₅ (OH)₈ (NO₃) 2.2 H₂O. *Acta Crystallogr B*. 1970;26(6): 860–863.
29. Petrov K, Lyubchova A, Markov L. Synthesis and thermal decomposition of magnesium hydroxide nitrates. *Polyhedron*. 1989;8(8): 1061–1067.
30. Rajamathi M, Kamath PV. Urea hydrolysis of cobalt (II) nitrate melts: synthesis of novel hydroxides and hydroxynitrates. *International Journal of Inorganic Materials*. 2001;3(7):901–906.
31. Strati A, Papoutsi Z, Lianidou E, Moutsatsou P. Effect of ellagic acid on the expression of human telomerase reverse transcriptase (hTERT) α+ β+ transcript in estrogen receptor-positive MCF-7 breast cancer cells. *Clin Biochem*. 2009;42(13–14):1358–1362.
32. Losso JN, Bansode RR, Trappey A. In vitro anti-proliferative activities of ellagic acid. *J Nutr Biochem*. 2004;15(11):672–678.
33. Kim S, Nishimoto SK, Bumgardner JD, Haggard WO, Gaber MW, Yang Y. A chitosan/[beta]-glycerophosphate thermo-sensitive gel for the delivery of ellagic acid for the treatment of brain cancer. *Biomaterials*. 2010;31(14):4157–4166.
34. Kim S, Liu Y, Gaber MW, Bumgardner JD, Haggard WO, Yang Y. Development of chitosan–ellagic acid films as a local drug delivery system to induce apoptotic death of human melanoma cells. *J Biom Mater Res B Appl Biomater*. 2009;90(1):145–155.
35. Morioka H, Tagaya H, Karasu M, Kadokawa J, Chiba K. Effects of zinc on the new preparation method of hydroxy double salts. *Inorg Chem*. 1999;38(19):4211–4216.
36. Hussein MZ, Hashim N, Yahaya AH, Zainal Z. Synthesis and characterization of [4-(2,4-dichlorophenoxybutyrate)-zinc layered hydroxide] nanohybrid. *Solid State Sciences*. 2010;12(5):770–775.
37. Nakayama H, Hatakeyama A, Tsuhako M. Encapsulation of nucleotides and DNA into Mg-Al layered double hydroxide. *Int J Pharm*. 2010;393(1–2):105–112.

38. Hussein MZ, Jaafar AM, Yahaya AH, Zainal Z. The effect of single, binary and ternary anions of chloride, carbonate and phosphate on the release of 2, 4-dichlorophenoxyacetate intercalated into the Zn-Al-layered double hydroxide nanohybrid. *Nanoscale Res Lett*. 2009;4(11):1351–1357.

39. Press RE, Hardcastle D. Some physico chemical properties of ellagic acid. *J Appl Chem*. 1969;19(9):247–251.

40. Gu Z, Thomas AC, Xu ZP, Campbell JH, Lu GQ. In vitro sustained release of LMWH from MgAl-layered double hydroxide nanohybrids. *Chem Mater*. 2008;20(11):3715–3722.

41. Panda HS, Srivastava R, Bahadur D. In-vitro release kinetics and stability of anticardiovascular drugs-intercalated layered double hydroxide nanohybrids. *J Phys Chem B*. 2009;113(45):15090–15100.

42. Dong L, Yan L, Hou WG, Liu SJ. Synthesis and release behavior of composites of camptothecin and layered double hydroxide. *J Solid State Chem*. 2010;183(8):1811–1816.

43. Kong X, Shi S, Han J, Zhu F, Wei M, Duan X. Preparation of glycy-l-tyrosine intercalated layered double hydroxide film and its in vitro release behavior. *Chem Eng J*. 2010;157(2–3):598–604.

44. Somchit N, Hassim SM, Samsudin SH. Itraconazole and fluconazole-induced toxicity in rat hepatocytes: a comparative in vitro study. *Hum Exp Toxicol*. 2002;21(1):43.

45. Marshall AD, Caldwell J. Influence of modulators of epoxide metabolism on the cytotoxicity of trans-anethole in freshly isolated rat hepatocytes. *Food Chem Toxicol*. 1992;30(6):467–473.

46. Somchit N, Wong CW, Zuraini A, et al. Involvement of phenobarbital and SKF 525A in the hepatotoxicity of antifungal drugs itraconazole and fluconazole in rats. *Drug Chem Toxicol*. 2006;29(3):237–253.

47. Marangoni R, Ramos LP, Wypych F. New multifunctional materials obtained by the intercalation of anionic dyes into layered zinc hydroxide nitrate followed by dispersion into poly(vinyl alcohol) (PVA). *J Colloid Interface Sci*. 2009;330(2):303–309.

48. Newman SP, Jones W. Comparative study of some layered hydroxide salts containing exchangeable interlayer anions. *J Solid State Chem*. 1999;148(1):26–40.

49. Xingfu Z, Zhaolin H, Yiqun F, Su C, Weiping D, Nanping X. Microspheric organization of multilayered ZnO nanosheets with hierarchically porous structures. *J Phys Chem C*. 2008;112(31):11722–11728.

50. Hasegawa M, Terauchi M, Kikuchi Y, et al. Deprotonation processes of ellagic acid in solution and solid states. *Monatsheftefür Chemie/Chemical Monthly*. 2003;134(6):811–821.

51. Yang JH, Han YS, Park M, Park T, Hwang SJ, Choy JH. New inorganic-based drug delivery system of indole-3-acetic acid-layered metal hydroxide nanohybrids with controlled release rate. *Chem Mater*. 2007;19(10):2679–2685.

52. Nayeem N, Karvekar MD. Isolation of phenolic compounds from the methanolic extract of Tectonagrandis. *Research Journal of Pharmaceutical, Biological and Chemical Sciences*. 2010;1(2):221–225.

53. Bindra RS, Satti NK, Suri OP. Isolation and structures of ellagic acid derivatives from Euphorbia acaulis. *Phytochemistry*. 1988;27(7):2313–2315.

54. Banait JS, Singh B, Kaur H. Electrochemical synthesis of zinc (II) phenoxides and their coordination compounds. *Portugaliae Electrochimica Acta*. 2007;25(4):435–442.

55. Rocca E, Caillet C, Mesbah A, Francois M, Steinmetz J. Intercalation in zinc-layered hydroxide: Zinc hydroxyheptanoate used as protective material on zinc. *Chem Mater*. 2006;18(26):6186–6193.

56. Sing KSW. The use of gas adsorption for the characterization of porous solids. *Colloids Surf*. 1989;38(1):113–124.

57. Hussein MZb, Hwa TK. Synthesis and Properties of Layered Organic–inorganic Hybrid Material: Zn-Al layered double hydroxide–dioctylsulfosuccinate nanocomposite. *J Nanopart Res*. 2000; 2(3): 293–298.

58. Smith RA. *Semiconductors*. 2nd vol. Cambridge, UK: Cambridge University Press; 1978.

59. Rousset J, Saucedo E, Lincot D. Extrinsic doping of electrodeposited ZnO films by chlorine for transparent conductive oxide applications. *Chem Mater*. 2009;21(3):534–540.